Separation of Spacecraft Noise from Geomagnetic Field Observations through Density-Based Cluster Analysis and Compressive Sensing

Alex Paul Hoffmann[1] and Mark B. Moldwin[2]

[1]University of Michigan
[2]University of Michigan-Ann Arbor

November 18, 2022

Abstract

Spacecraft equipped with magnetometers provide useful magnetic field data for a variety of applications such as monitoring the Earth's magnetic field. However, spacecraft electrical systems generate magnetic noise that interfere with geomagnetic field data captured by magnetometers. Traditional solutions to this problem utilize mechanical booms to extend magnetometers away from noise sources. This solution can increase design complexity, cost, and introduce boom deployment risk. If a spacecraft is equipped with multiple magnetometers, signal processing algorithms can be used to compare magnetometer measurements and remove stray magnetic noise signals. We propose the use of density-based cluster analysis to identify spacecraft noise signals and compressive sensing to separate spacecraft noise from geomagnetic field data. This method assumes no prior knowledge of the number, location, or amplitude of noise signals, but assumes that they are independent and have minimal overlapping spectral properties. We demonstrate the validity of this algorithm by separating high latitude magnetic perturbations recorded by SWARM from noise signals in simulation and in a laboratory experiment using a mock CubeSat apparatus. In the case of more noise sources than magnetometers, this problem is an instance of Underdetermined Blind Source Separation (UBSS). This work presents a UBSS signal processing algorithm to remove spacecraft noise and eliminate the need for a mechanical boom.

Posted on 18 Nov 2022 — CC-BY-NC 4 — https://doi.org/10.1002/essoar.10510730.1 — This a preprint and has not been peer reviewed. Data may be preliminary.

Separation of Spacecraft Noise from Geomagnetic Field Observations through Density-Based Cluster Analysis and Compressive Sensing

Alex Paul Hoffmann[1], **Mark B. Moldwin**[1]

[1]Climate and Space Sciences and Engineering, University of Michigan, Ann Arbor, Michigan

Key Points:

- We present the first use of compressive sensing with cluster analysis to separate spacecraft noise from geomagnetic field data.
- We demonstrate the separation of phase-delayed signals in simulation as well as in a laboratory experiment using SWARM residual geomagnetic field data.
- The method enables high fidelity magnetic field measurements from resource constrained and magnetically noisy spacecraft such as boomless CubeSats.

Corresponding author: Alex Paul Hoffmann, `aphoff@umich.edu`

Abstract

Spacecraft equipped with magnetometers provide useful magnetic field data for a variety of applications such as monitoring the Earth's magnetic field. However, spacecraft electrical systems generate magnetic noise that interfere with geomagnetic field data captured by magnetometers. Traditional solutions to this problem utilize mechanical booms to extend magnetometers away from noise sources. This solution can increase design complexity, cost, and introduce boom deployment risk. If a spacecraft is equipped with multiple magnetometers, signal processing algorithms can be used to compare magnetometer measurements and remove stray magnetic noise signals. We propose the use of density-based cluster analysis to identify spacecraft noise signals and compressive sensing to separate spacecraft noise from geomagnetic field data. This method assumes no prior knowledge of the number, location, or amplitude of noise signals, but assumes that they are independent and have minimal overlapping spectral properties. We demonstrate the validity of this algorithm by separating high latitude magnetic perturbations recorded by SWARM from noise signals in simulation and in a laboratory experiment using a mock CubeSat apparatus. In the case of more noise sources than magnetometers, this problem is an instance of Underdetermined Blind Source Separation (UBSS). This work presents a UBSS signal processing algorithm to remove spacecraft noise and eliminate the need for a mechanical boom.

Plain Language Summary

Magnetometers are instruments designed to measure magnetic fields. They are used for a variety of purposes such as monitoring the magnetic field of the Earth from spacecraft. Spacecraft systems such as solar panels and reaction wheels generate magnetic noise that interferes with magnetometer readings. If the spacecraft has multiple magnetometers, each noise source will have a different magnitude at each magnetometer depending on the location of the noise source. The system which describes the magnitude of each noise source at each magnetometer is called a mixing matrix. We propose the use of unsupervised machine learning to estimate the mixing matrix. Once the mixing matrix is estimated, the Earth's magnetic field can be separated from spacecraft magnetic noise using a method called Compressive Sensing.

1 Introduction

Spacecraft equipped with magnetometers can be used to capture in situ measurements of magnetic phenomena in the geospace environment. These measurements are necessary to answer key questions about the nature of the Earth's magnetosphere and its interaction with interplanetary magnetic fields. Understanding how the heliosphere directs the flow of energy, mass, and momentum between the Sun and Earth is critical for a number of applications such as space weather modeling, space exploration, and climate science. A number of missions use spacecraft equipped with magnetometers to measure magnetic fields. For example, The European Space Agency's SWARM mission uses a constellation of three satellites to provide high fidelity magnetic field measurements used to model the Earth's magnetic field and study the Earth's dynamo (Fratter et al., 2016). Magnetometers provide invaluable data for space science research, however, the quality of the data is often limited by magnetic noise generated by the spacecraft. Electrical systems onboard a spacecraft generate stray magnetic fields that interfere with magnetic field measurements germane to scientific investigation. The presence of these stray magnetic fields is a significant obstacle for missions which utilize magnetic field data (Russell, 2004; Ludlam et al., 2009).

On satellites, stray magnetic fields can be generated by subsystems such as solar panels, reaction wheels, battery currents, and magnetorquers. Satellite magnetometers are typically fixed at the end of a mechanical boom to reduce the magnitude of noise generated by the spacecraft. For example, the mission SWARM uses two magnetometers mounted on a 4.3 meter boom (McMahon et al., 2013). However, the use of a boom is not always possible in designs such as rovers and CubeSats where gravity and cost are limiting factors. Booms are also problematic on non-magnetic spacecraft such as DMSP, which are equipped with a tri-axial fluxgate magnetometer on the end of a telescoping boom, but still faces issues with spacecraft noise (Kilcommons et al., 2017).

The use of a single magnetometer on a spacecraft requires characterization of the spacecraft's magnetic signature in order to remove stray magnetic fields. In the case of the spacecraft Cassiope, a software update changed the behavior of the spacecraft's fluxgate magnetometer (MGF). Special spacecraft maneuvers to decrease the spacecraft's noise signature were required in order to recalibrate the MGF (Miles et al., 2019). Algorithms to autonomously identify spacecraft noise would allow Cassiopie to do in situ MGF calibration without special spacecraft maneuvers.

In spacecraft with multiple magnetometers, the traditional way to cancel stray magnetic field noise is to perform gradiometry. Gradiometry is a technique which compares magnetometer signals and calculates the gradient of between them (Ness et al., 1971; Ream et al., 2021). The calculated gradient is used to identify and suppress noise signals. This method requires spatial knowledge of the magnetometers and assumes that the magnetic noise sources are dipole structured. More recently, Imajo et al. (2021) proposed the use of Independent Component Analysis (ICA) to separate geomagnetic field data, captured by the satellite Michibiki-1, from stray magnetic field noise. Imajo et al. (2021) apply ICA by assuming that there are M-1 noise signals recorded by M magnetometers. The satellite, Michibiki-1, has one magnetometer mounted on the end of a short boom, and another mounted at the base of the boom on the spacecraft. Because there are two magnetometers, Imajo et al. (2021) assume a single geomagnetic field and noise signal for each cartesian axis. This algorithm separates signals based on statistical independence, and works well when the number of noise sources is not more than the number of magnetometers (Naik & Kumar, 2009). Spacecraft typically have an abundance of noise generating electrical equipment, so this condition is rarely met. Sheinker and Moldwin (2016) proposed an analytical method which uses a pair of magnetometers to adaptively cancel magnetic interference without prior knowledge of the noise signal. This method is designed for the case in which a single noise source is present, and does not account for the presence of multiple noise sources. Although, the method may be applied to remove multiple noise sources by adding more magnetometers. Other methods employ state estimation of the magnetic fields generated by spacecraft subsystems by examining spacecraft housekeeping data. Deshmukh et al. (2020) uses a supervised machine learning algorithm in order to estimate the transfer function of housekeeping currents to stray magnetic fields. Total knowledge of a spacecraft's magnetic signature would allow for perfect interference cancellation, however, housekeeping telemetry provides an incomplete image of a spacecraft's current distribution. For low cost applications with a large number of spacecraft, such as CubeSat constellations, it is advantageous to use an algorithm that does not rely on prior knowledge of the spacecraft's magnetic signature or requires human analysis.

In this work, we present the application of the unsupervised machine learning algorithm, Density Based Spatial Clustering of Applications with Noise (DBSCAN), and compressive sensing to separate the geomagnetic field signal from stray magnetic field noise. The separation of geomagnetic signals from stray magnetic fields is an instance of Underdetermined Blind Source Separation (UBSS). UBSS is a class of problems in which there are m listeners, $B(k) \in \mathbb{C}^m$, and n noises sources, $S(k) \in \mathbb{C}^n$, such that $m < n$. The source signals combine in an unknown mixing matrix $\boldsymbol{K} \in \mathbb{C}^{m \times n}$. UBSS is a topic that has been thoroughly researched in other fields such as acoustics and radar signal processing. The system used to model UBSS is defined by the following relationship.

$$\mathbf{B(k)} = \mathbf{KS(k)} \tag{1}$$

In the field of acoustics, this problem is famously referred to as the cocktail party problem. In the cocktail party problem, there is a room full of people each having conversations. An array of microphones is placed in the room to record the concurrent conversations. The microphone recordings are then used to separate each individual voice. Guo et al. (2017) demonstrate the separation of four human voices using three microphones. He et al. (2021) also demonstrate the separation of six flutes recorded by three microphones using the DBSCAN algorithm.

Due to the spatial structure of magnetic fields, the same algorithms developed to solve the cocktail party problem can not be directly applied to magnetic noise cancellation. A magnetic noise signal, s(t), will appear to have a different phase and magnitude at each magnetometer depending on the radial distance and magnetic latitude of the magnetometer with respect to the noise source. This structure will change depending on the geometry of the noise source. In magnetic underdetermined blind source separation, the mixing matrix, K, represents the gain and phase of each signal at each magnetometer. DBSCAN is used to estimate the mixing matrix, K. Once K is known, compressive sensing is used to restore the geomagnetic field signal from the noisy magnetometer data.

We present two experiments to validate this algorithm. The first experiment separates four computer-simulated noise signals from an ambient magnetic field signal. The second experiment separates the same ambient magnetic field signal using real magnetic field data recorded using an experimental CubeSat apparatus with copper coil generated signals and three PNI RM3100 magnetometers (Regoli et al., 2018). The aim of this work is to develop a robust signal processing algorithm to remove spacecraft noise and eliminate the need for a mechanical boom. This work focuses on developing a noise cancellation algorithm for geomagnetic field data, but can also be applied to remove noise in measurements of planetary magnetospheres and interplanetary magnetic fields.

2 Methodology

We apply an iterative approach to identifying spacecraft noise and reconstructing the geomagnetic field signal. Noise signals may be present at different orders of magnitude or frequency spectra. In order to increase the discoverability of a noise signal, we iteratively look at limited frequency bands by using a bandpass filter on the input signals to analyze the signals over a smaller frequency space. Noise signals are identified by transforming the magnetometer data into a sparse domain and clustering the transformed data. After the noise signals are identified, we use compressive sensing to reconstruct the geomagnetic field with the noise signals removed.

2.1 Signal Preprocessing

The separation of magnetic field signals from stray magnetic fields is analogous to a problem thoroughly researched in other fields such as acoustics and is called Underdetermined Blind Source Separation (UBSS). This problem has been heavily investigated for microphone and radar arrays, but the unique structure of a magnetic dipole introduces new complications which have not been well-researched. The placement of magnetometers at different magnetic latitudes makes the magnetic noise signal appear to be phase-delayed, despite mixing instantaneously. As a result, time-frequency domain mixing model, B(t,k) = KS(t,k), can be represented as the following system:

$$\begin{bmatrix} B_1(t,k) \\ B_2(t,k) \\ \vdots \\ B_m(t,k) \end{bmatrix} = \begin{bmatrix} 1 & k_{12}\angle\phi_{12} & k_{13}\angle\phi_{13} & ... & k_{1n}\angle\phi_{1n} \\ 1 & k_{22}\angle\phi_{22} & k_{23}\angle\phi_{23} & ... & k_{2n}\angle\phi_{2n} \\ \vdots & \vdots & \vdots & \ddots & \vdots \\ 1 & k_{m2}\angle\phi_{m2} & k_{m3}\angle\phi_{m3} & ... & k_{mn}\angle\phi_{mn} \end{bmatrix} \begin{bmatrix} S_1(t,k) \\ S_2(t,k) \\ \vdots \\ S_n(t,k) \end{bmatrix} \tag{2}$$

In this mixing system, the geomagnetic source signal we seek to recover, S_1(t,k), is assumed to be identical at each magnetometer a priori. In the geospace environment, this allows us to observe phenomena such as ULF waves which have frequencies less than 5 Hz (Jacobs et al. 1964). The phases, ϕ_{ij}, in the mixing matrix, K, account for the difference of a signal seen by magnetometers at different magnetic latitudes.

Once the magnetometer signals, b(t), have been filtered through a bandpass, they are transformed into the Time-Frequency (TF) domain using a Fourier transform in order to increase signal sparsity. Sparsity is a precondition of both mixing matrix estimation and compressive sensing, however, spacecraft noise signals are not often sparse in the time domain. Typically, the Short-Time Fourier Transform (STFT) is used because signals that are present in multiple time windows will provide more data points to be clustered. In this work, we use the Non-Stationary Gabor Transform (NSGT) to transform magnetometer signals into the Time-Frequency domain. NSGT has advantages over the STFT because it allows the user to evolve the window size with respect to frequency (Jaillet et al., n.d.). As a result, high and low frequencies are not limited to the same Window size, and frequency resolution is greatly increased. NSGT also improves the representation of transient signals with respect to traditional transforms. We perform the Non-Stationary Gabor Transform to obtain the UBSS model B(t,k) = KS(t,k). The mixing system of a sparse time-frequency bin where only the signal, S_j(t,k), is present can be defined by a single mixing vector:

$$\begin{bmatrix} \|B_1(t,k)\| \\ \|B_2(t,k)\| \\ \vdots \\ \|B_m(t,k)\| \end{bmatrix} = \begin{bmatrix} k_{1j} \\ k_{2j} \\ \vdots \\ k_{mj} \end{bmatrix} \|S_j(t,k)\| \tag{3}$$

Equation (3) can be rewritten element-wise as:

$$\|S_j(t,k)\| = \frac{\|B_1(t,k)\|}{k_{1j}} = \frac{\|B_2(t,k)\|}{k_{2j}} = ... = \frac{\|B_m(t,k)\|}{k_{mj}} \tag{4}$$

Equation (4) is equivalent to the symmetric form of a line with slope defined by the mixing vector of the noise signal. In order to exploit this relationship, we define a time-frequency space $\mathbf{H} \in \mathbb{R}^{2m}$ in which each phase and magnitude of the m magnetometer signals are an axis. Sparse TF points will draw straight lines through the origin in the **H**-domain with a slope proportional to the signal's mixing vector.

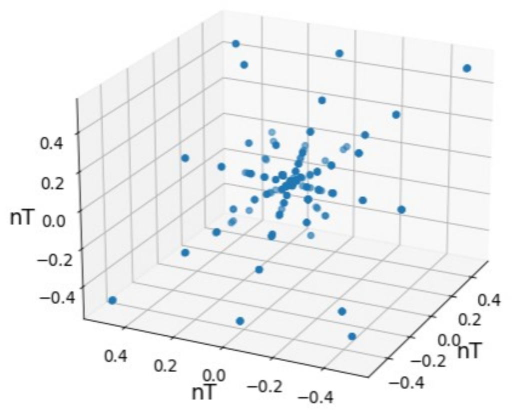

Figure 1. Six computer generated signals plotted against each other in the frequency domain.

2.2 Mixing Matrix Estimation

The slope of the lines drawn through the **H**-domain are not easily clusterable in their current form as a collection of scattered data points. We transform the scattered data points in **H**-domain into a clusterable form by projecting the magnitude subspace onto a unit hypersphere. Figure 2 shows the projected data points of the scattered data in Figure 1.

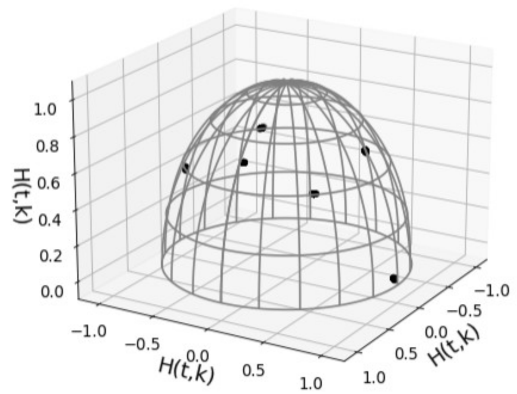

Figure 2. Six computer-generated signals projected onto a half-unit hypersphere in the H-Domain.

The **H**-domain magnitude subspace is projected onto a half-unit hypersphere using the following equation.

$$B^*(t,k) = \frac{|B(t,k)|}{\|B(t,k)\|} \tag{5}$$

The majority of the frequency space is filled with negligible energy points that will project randomly onto the unit hypersphere (Sun et al., 2016). We attempt to cleanse the data of these points using a magnitude filter with $\lambda \in (0,1)$:

$$|B(t,k)| > \lambda \cdot \max(|B(t,k)|) \tag{6}$$

The projected data points form tightly clustered groups on the unit hypersphere that allow us to discover the relative gain between noise signals at different magnetometers. However, we need to find the relative phases between noise signals at magnetometers of different magnetic latitudes. To account for this we join each projected time-frequency point to its relative argument. The relative argument is defined by the following transformation:

$$\arg B(t,k) = \{\, \arg B_j(t,k) - \arg\left(B_0(t,k) \mid j \in [0,m]\,\right\} \tag{7}$$

Using the result of Equation 7, we define a new data format H(t,k) by concatenating the projected magnitude data with the argument of the time-frequency data.

$$H(t,k) = (B^*(t,k), \arg\left(B(t,k)\right)) \tag{8}$$

The magnetometer data, H(t,k), are now in a format that can be clustered to discover the gain and phase of each signal described in the mixing matrix, K. Figure 3 shows an example of signal clusters in a two magnetometer system.

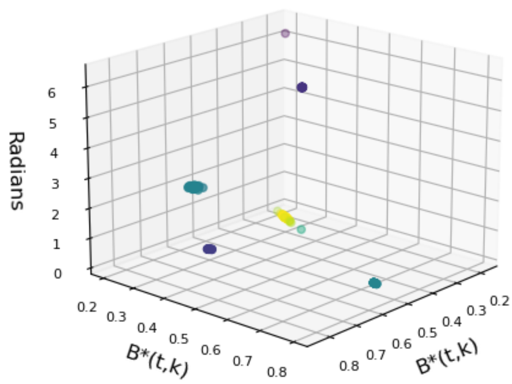

Figure 3. Five simulated signals recorded by two magnetometers in the H-Space. The horizontal axes are the magnitudes projected onto a unit hypersphere. The vertical axis is the relative phase found by Equation 7.

Now that the projected magnitude and relative phases are joined, a variety of clustering algorithms can be applied to find the mixing matrix, K. In this work, we use the Density Based Spatial Clustering for Applications with Noise (DBSCAN) algorithm because it does not require user input to discern the number of clusters present, and it will ignore noise points (Ester et al. 1996). DBSCAN has two essential parameters, *eps* and *minPts*, that allow this functionality. The maximum distance for two points to become neighbors is the value, *eps*. If a point has *minPts* number of neighbors, it is called a core point. Core points are used to define each cluster. If a point is more than *eps* distance away from any point in a cluster, it is labeled as noise. We use DBSCAN to cluster H(t,k) and use each cluster's centroid as the noise signal's mixing vector.

2.3 Signal Reconstruction

Compressive sensing is a method used to reconstruct sparse signals with a sampling rate below two times a signal's bandwidth (Baraniuk, 2007). Reconstructing a signal of length N from a sampled signal of length M, where $M < N$, is an analogous problem to Underdetermined Blind Source Separation. Ordinarily, the system $b = Ks$, where K is a wide matrix, has infinitely many solutions because if $b = Ks$ is a solution, $b = K(s+s')$ is also a solution for any vector s' in the null space of K. Compressive sensing can exactly recover sparse signals and approximate near-sparse signals through minimizing the L1 norm of S with respect to $b-Ks < \varepsilon$. The algorithm works with O(N^3) complexity.

We use CVXPY, A Python-Embedded Modeling Language for Convex Optimization (Diamond & Boyd, n.d.), to reconstruct the signals with the estimated mixing matrix, K. The constraint used to recover the signal, s, from b is:

$$\begin{aligned} &\text{Minimize} && \|s\|_1 \\ &\text{Subject to} && Ks = b \end{aligned} \tag{9}$$

This system is solved using the convex optimization algorithm, Embedded Conic Solver (Domahidi et al., 2013).

3 Experimental Data and Results

We test the proposed method of signal and noise separation through two experiments. The first experiment demonstrates the separation of SWARM magnetic field data from computer simulated signals using virtual magnetometers. The second experiment demonstrates the separation of SWARM magnetic field data from real magnetic noise signals generated with copper coils. The coil-generated magnetic fields were measured using the PNI RM3100 magnetometer and a mock CubeSat described by Deshmukh et al. (2020).

Figure 5 details the process of identifying noise signals and reconstructing the ambient magnetic field. First (i), the signal offsets are subtracted to center the signals around 0 nT. Second (ii), the signals are bandpassed so the algorithm can analyze a more limited frequency range. Third (iii), the signals are transformed into the time-frequency domain using the Non-Stationary Gabor Transform to increase signal sparsity. Fourth (iv), low energy points are filtered out using Equation 6. Fifth (v), the signals are transformed into H(t,k) by projecting the magnitude, $|B(t,k)|$ onto the unit hypersphere and concatenating it with the phase, $\arg B(t,k)$, via Equations 5, 7, and 8. Sixth (vi), the data, H(t,k), are clustered using DBSCAN and the cluster centroids are found. This process loops back to step ii until the whole frequency spectrum has been swept. Finally, in the last step (vi), compressive sensing is used to reconstruct the ambient magnetic field. The minimum magnitude, λ in step iv, and the parameters eps and MinPts in step vi may need to be adjusted depending on the length and magnitude of the signals being analyzed.

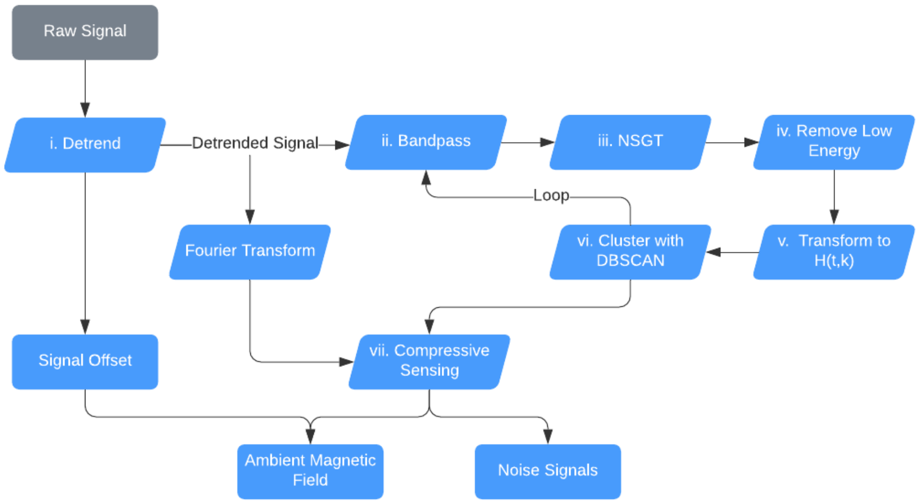

Figure 4. Flow of processes involved in using cluster analysis to discover noise signals and compressive sensing to separate the ambient magnetic field from noise signals.

We evaluate the separation of noise signals via three metrics. The first metric is the Pearson Correlation Coefficient. This measurement gives the covariance between the normalized input and recovered signals.

$$\rho = \frac{\sum_{i=0}^{N-1}(x_i - \bar{x})(y_i - \bar{y})}{\sqrt{\sum_{i=0}^{N-1} |(x_i - \bar{x})|^2 \sum_{i=0}^{N-1} |(y_i - \bar{y})|^2}} \tag{10}$$

The second metric evaluated is the root mean squared error (RMSE). This metric is proportional to the magnitude of the squared error. As a result, the RMSE is very sensitive to large errors.

$$RMSE = \sqrt{\frac{\sum_{i=0}^{N-1}(x_i - y_i)^2}{N}} \tag{11}$$

The final metric is the normalized RMSE (NRMSE). This metric yields the RMSE as a percentage of the magnitude of the signal being measured. It is used to compare the relative error between signals on different orders of magnitude.

$$NRMSE = \frac{RMSE}{|y_{max}|} \tag{12}$$

3.1 Experiment 1: Computer Simulation

In this experiment, we use four simulated noise signals, $s(t) \supset [s_2(t), s_3(t), s_4(t), s_5(t)]$, and three virtual magnetometers $b(t) = Ks(t) = [b_1(t), b_2(t), b_3(t)]$. The signal, $s_1(t)$, is residual magnetic field data created by subtracting data generated by the IGRF model from SWARM magnetic field data. This process leaves only magnetic perturbations present in the magnetosphere. The magnetic perturbation data we use were measured by the SWARM A satellite on March 17th, 2015 between 8:53 and 8:55 UTC. This part of the orbit passes between the 69th and 76th parallel south and was selected to capture perturbations in the southern auroral zone. The proposed algorithm detailed in Figure 4 is tested on 100 seconds of data, although it may be applied to a signal of any length provided that there are enough data points to cluster. The signals are combined through the complex mixing matrix in Equation 13 with phases given in radians.

$$K = \begin{bmatrix} 1\angle 0 & 0.83\angle 0 & 0.56\angle 0 & 0.68\angle 0 & 0.30\angle 0 \\ 1\angle 0 & 0.50\angle 1.57 & 0.79\angle 0.523 & 0.29\angle 2.35 & 0.30\angle 0.314 \\ 1\angle 0 & 0.24\angle 1.04 & 0.24\angle 1.04 & 0.68\angle 3.14 & 0.90\angle 0.523 \end{bmatrix} \tag{13}$$

The values in the first column represent the ambient magnetic field signal which appears identically at every magnetometer. Figure 5 shows the five source signals used in this simulation. Two of the noise signals are sine waves with frequencies of 2 Hz and 5 Hz. Sine waves are sparse signals that can be represented by a single point in the frequency domain. This makes them easily identifiable by cluster analysis. The two remaining noise signals used are a sawtooth wave with a frequency of 0.7 Hz, and a square wave with a frequency of 3.0 Hz. These signals inhabit a broad frequency spectrum and diminish the sparsity of the mixed signals.

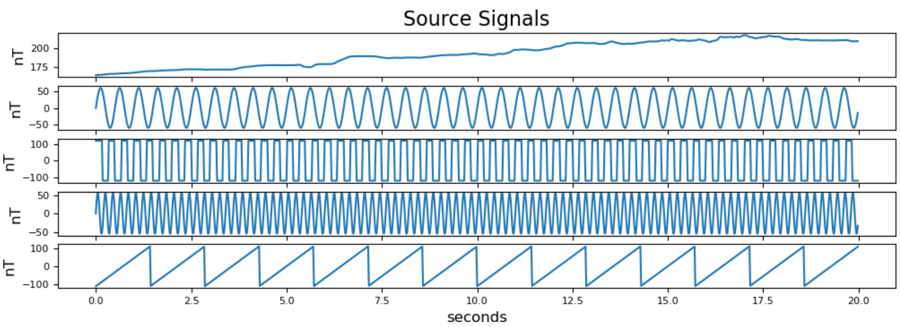

Figure 5. Five computer generated source signals.

The signals are combined in the mixing system $b(t) = Ks(t)$ with the mixing matrix K from equation 13. The resulting signals are sampled by the virtual magnetometers at a rate of 50 samples per second. A random normal signal with a standard deviation of 6 nT is added to each virtual magnetometer in order to simulate instrument noise. Figure 6 shows the sampled signals.

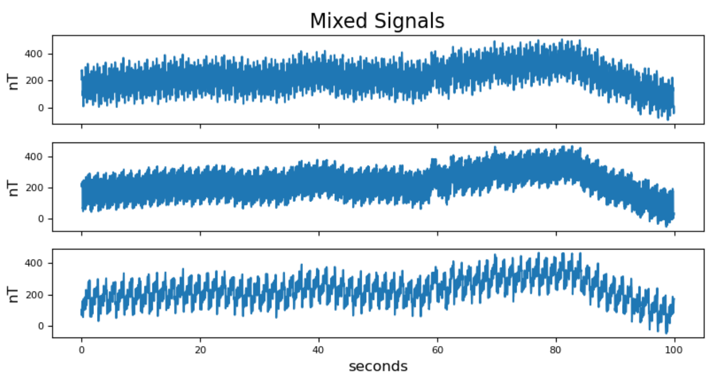

Figure 6. Three magnetometer signals created by mixing the five source signals in Figure 5.

Following the procedure in Figure 4, the signals were detrended and bandpassed with frequency ranges of [0.01 Hz, 2.12 Hz] and [0.15 Hz, 25 Hz]. Overlapping frequency ranges are analyzed to discover signals that may appear in multiple frequency bands. The signals were then transformed into the Time-Frequency domain using the NSGT. The NSGT is a type of constant-Q transform, so it requires the parameter Q which specifies window size. In this experiment, we used $Q = 20$. In step 4, low energy points were removed using a $\lambda = 0.01$. The resulting data were transformed into H(t,k) and clustered by DBSCAN with parameters $eps = 0.3$ and $MinPts = 3$. These parameters were optimized experimentally using trial and error, however it may be possible to automate parameter selection based on the signals being analyzed. With this configuration, DBSCAN discovered the five clusters corresponding to each noise source. The clusters, shown below in the columns of $\hat{K}$, closely match the original mixing matrix.

$$\hat{K} = \begin{bmatrix} 1\angle 0 & 0.83\angle 0.00 & 0.57\angle 0.00 & 0.62\angle 0.00 & 0.308\angle 0.00 \\ 1\angle 0 & 0.50\angle 1.57 & 0.70\angle 0.31 & 0.33\angle 2.63 & 0.31\angle 0.33 \\ 1\angle 0 & 0.24\angle 1.02 & 0.39\angle 0.56 & 0.70\angle -3.1 & 0.90\angle 0.51 \end{bmatrix} \tag{14}$$

Finally, in step 7, the mixed signals were separated by compressive sensing using the recovered mixing matrix, $\hat{K}$, in Equation 15. The data, H(t,k), are discarded and the raw Fourier transform of the mixed signals is separated using the ECOS algorithm. The reconstructed SWARM perturbation signal is shown in Figure 7 with the original signal overlayed.

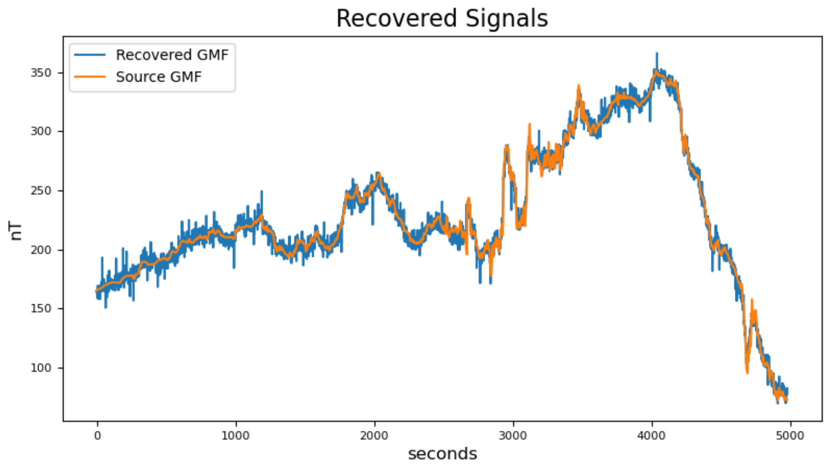

Figure 7. True magnetic perturbation signal in orange versus the recovered magnetic perturbation signal in blue. The signal was reconstructed using the mixed signals in Figure 6 sampled at a rate of 50 Hz.

The reconstructed ambient magnetic field signal resembles the original signal with some additional error. In order to evaluate the reconstruction noise, the Pearson Correlation Coefficient, RMSE, and NRMSE of each source signal are calculated. The ambient magnetic field was reconstructed with a RMSE of 5.79 nT. The results for each source signal are shown in the following table.

Metrics					
	SWARM	Sine A	Square	Sine B	Sawtooth
ρ	0.9950	0.9954	0.9972	0.9996	0.8868
RMSE	5.79 nT	4.165 nT	17.00 nT	1.297 nT	33.49 nT
NRMSE	1.33%	6.94%	21.1%	2.26%	30.45%

3.2 Experiment 2: Magnetic-Coil Generated Signal Separation

In this experiment, we demonstrate the utility of the proposed algorithm on real magnetic field data. We use three PNI RM3100 magnetometers to record copper coil-generated noise signals. Four copper coils are driven by signal generators to create the source signals, $s(t) \supset [s_2(t), s_3(t), s_4(t), s_5(t)]$. The signals are combined in the unknown mixing system, $b(t) = Ks(t) = [b_1(t), b_2(t), b_3(t)]$. The SWARM residual magnetic field data, which is used in experiment one, is added to each magnetometer recording to generate the ambient magnetic field signal, $s_1(t)$.

The proposed algorithm detailed in Figure 4 is tested on 100 seconds of recorded data. The signals, $s_2(t)$ and $s_3(t)$, are sine waves with frequencies of 0.4 Hz and 0.8 Hz. The signals, $s_4(t)$ and $s_5(t)$, are square waves with frequencies of 1 Hz and 2 Hz. The three PNI RM3100 magnetometers and four copper coils are placed on the CubeSat apparatus as shown in Figure 8. Due to the location and orientation of the four copper coils and three magnetometers, each noise signal will appear at each magnetometer with a different magnitude and magnetic latitude induced phase. Additionally, this experiment was performed in a copper room lined with mu-metal in order to screen out magnetic fields from the surrounding environment.

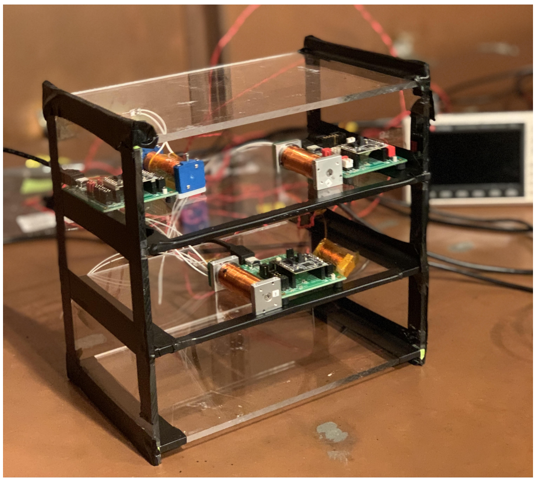

Figure 8. Mock CubeSat Apparatus with three PNI RM3100 Magnetometers and four copper coils driven by signal generators. The Apparatus is placed inside a mu-metal lined copper room that acts as a large magnetic shield can.

The PNI RM3100 is a magneto-inductive magnetometer that measures the magnetic field by counting hysteresis loops with a comparator circuit, called a Schmitt Trigger, in an ASIC. The ASIC records magnetic field measurements by adding to a register every time the Schmitt trigger is saturated. This measurement renders the magnetic field when integrated with respect to time. The ASIC has a cycle count register that controls how many clock cycles pass between integrations. The error of the magnetometer will change with respect to the cycle count. In this experiment, each magnetometer is sampled at a rate of 50 Hz with a cycle count of 200 cycles. The PNI RM3100 is rated to have an error of 6 nT in this configuration. The mixed signals recorded by the PNI RM3100 magnetometers are shown in Figure 9 below.

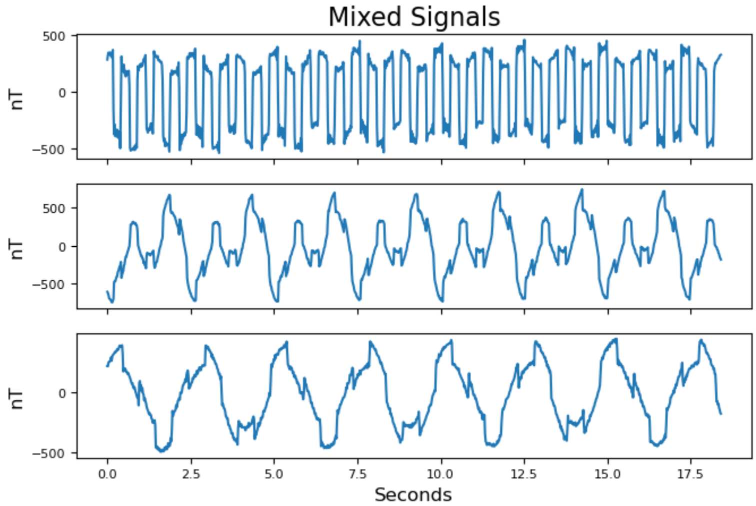

Figure 9. Three mixed signals recorded by PNI RM3100 magnetometers. The five signals present are two sine waves, two square waves, and the added residual magnetic field data.

The algorithm was run on this data following the same steps as in Figure 4 and section 3.1. The signals were detrended and bandpassed with frequency ranges of [0.01 Hz, 0.51 Hz], [0.07 Hz, 3.76 Hz], and [0.51 Hz, 25 Hz]. The signals were then transformed into the Time-Frequency domain using the NSGT with a quality factor of $Q = 10$. In step 4, low energy points were removed using a $\lambda = 0.09$. The resulting data were transformed into H(t,k) and clustered by DBSCAN with parameters $eps = 0.3$ and $MinPts = 3$. DBSCAN discovered the following five clusters shown below in the columns of $\hat{K}$.

$$\hat{K} = \begin{bmatrix} 1\angle 0 & 0.023\angle 0 & 0.22\angle 0 & 0.93\angle 0 & 0.02\angle 0 \\ 1\angle 0 & 0.55\angle 1.31 & 0.97\angle 3.09 & 0.35\angle 3.04 & 0.04\angle 6.04 \\ 1\angle 0 & 0.79\angle 4.58 & 0.001\angle 2.94 & 0.15\angle 0.255 & 0.82\angle 2.84 \end{bmatrix} \tag{15}$$

The PNI RM3100 magnetometer was experimentally found to have a lower noise floor when sampled at a higher rate and decimated to a lower rate versus only being sampled at a lower rate. We evaluated this effect by testing step 7, signal reconstruction, on the original 50 Hz data, 10 Hz and 1 Hz data attained through downsampling, and 50 Hz data averaged with a moving mean (N = 10). These signals were separated via compressive sensing using the recovered mixing matrix, $\hat{K}$, in Equation 15. The four reconstructed noise signals from the 50 Hz raw data are shown in Figure 10.

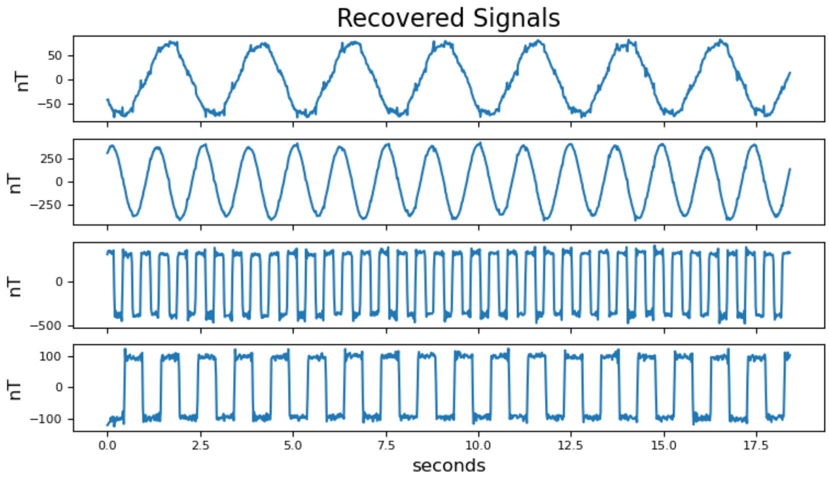

Figure 10. Reconstructed Sine and Square wave signals from 50 Hz mixed signals in Figure 9.

The reconstructed coil-generated signals closely resemble square and sine waves with some additional noise. The recovered residual magnetic field data are shown in Figure 11. The recovered signal is overlayed with the true residual magnetic field signal. The residual data in Figure 11 was reconstructed using the mixed signals decimated to a sampling rate of 10 Hz.

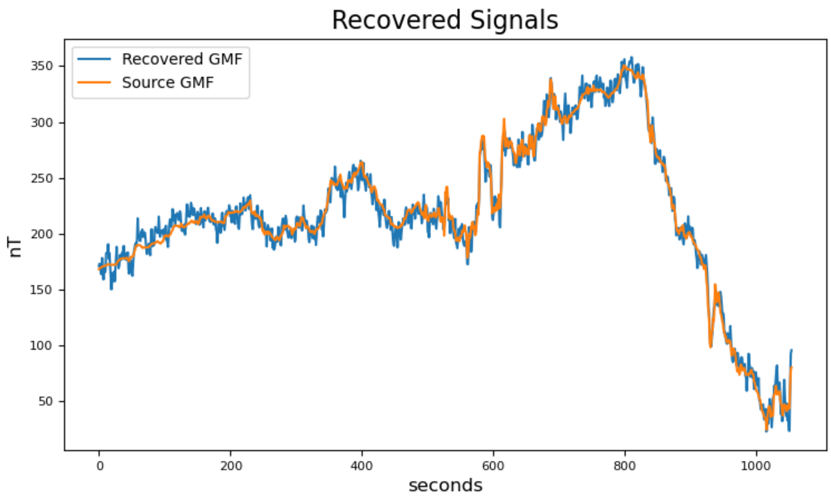

Figure 11. True magnetic perturbation data in orange versus the recovered magnetic perturbation signal in blue. The signal was reconstructed using the mixed signals in Figure 9 decimated to a sampling rate of 10 Hz.

The reconstructed signal closely follows the true geomagnetic perturbation signal with some high frequency noise present. As a result of the geomagnetic field signal being artificially inserted into the magnetometer readings, we are able to calculate the RMSE and Pearson Correlation Coefficient with respect to the original signal. The results for the original, decimated, and moving-mean signals are shown in the following table.

Metrics				
	50 Hz	10 Hz	1 Hz	Moving Mean (N=10)
ρ	0.979	0.993	0.98	0.995
RMSE	14.7 nT	5.92 nT	3.73 nT	6.91 nT
NRMSE	3.37%	1.36%	0.85%	1.58%

4 Discussion

In this study, we introduced a signal processing algorithm based on UBSS and demonstrated the separation of magnetic noise from geomagnetic field data. In the first experiment, we separated four simulated noise signals from SWARM residual magnetic field data. The noise signals contained both sparse sine wave signals and wideband sawtooth and square wave signals. The algorithm was able to restore the residual magnetic field signal with a correlation coefficient of $\rho = 0.9950$ and RMSE of 5.79 nT. This experiment was repeated without artificial instrument noise and yielded a RMSE of 3.88 nT for the ULF signal. In the second experiment, we created four magnetic noise signals using copper coils to generate real magnetic field data and placed PNI RM3100 magnetometers within the bus of a mock CubeSat apparatus. The same SWARM magnetic residual data were artificially inserted into the magnetometer measurements. This experiment mimicked the computer simulated experiment, with two sparse noise signals and two wideband noise signals. With a sampling rate of 50 Hz, the SWARM data had a reconstruction error of 14.7 nT using real magnetic field data as opposed to 5.79 nT in simulation. The signal separation algorithm was executed using several additional preprocessing techniques such as decimating the sampling rate and applying a moving mean to the magnetometer data. The lowest RMSE of 3.73 nT was achieved by decimating the sample rate to 1 Hz. At 1 Hz, the PNI RM3100 magnetometer is rated to have a measurement error of 1.2 nT due to instrument noise. This result places the reconstruction error near the noise floor of the magnetometer. These results show that the proposed UBSS algorithm is effective at removing spacecraft noise from magnetic field data.

In general, it is not feasible to adaptively cancel spacecraft noise when a single magnetometer is used. Adaptive noise cancellation requires the removal of noise signals that are time variable. The use of a single magnetometer requires that spacecraft noise be carefully characterized before launch. Otherwise, a change in spacecraft behavior may require special maneuvers to re-characterize noise signatures in situ (Miles et al., 2019). The use of multiple magnetometers allows for the discovery of noise signals through the comparison of magnetometer data. Sheinker and Moldwin (2016), Deshmukh et al. (2020), and Imajo et al. (2021) each propose algorithms for noise cancellation using multiple magnetometers. The algorithm proposed by Sheinker and Moldwin (2016) is effective at removing a single noise signal, but is not designed for multiple noise signals. Imajo et al. (2021) propose the use of ICA which is also limited by how many noise signals it can remove. ICA requires that the number of noise signals be less than the number of magnetometers. Spacecraft contain many electrical systems that could generate magnetic interference, so this condition is rarely met. The advantage of the proposed UBSS algorithm over Imajo et al. (2021) and Sheinker and Moldwin (2016) is that it can cancel noise signals in an underdetermined system. This means that there are more noise signals present than magnetometers. This property of the algorithm provides the flexibility necessary to be applied to many different spacecraft without prior characterization of spacecraft noise. The algorithm also does not require knowledge of magnetometer location and orientation. Finally, Deshmukh et al. (2020) designed a state estimation algorithm to transform housekeeping data to magnetic noise signals. Housekeeping currents provide an incomplete mapping of the distribution of currents within a spacecraft. The advantage of the proposed UBSS algorithm over this approach is that it is a blind signal processing algorithm. It requires no housekeeping data to identify and remove noise signals.

The proposed algorithm functions on the assumption that the noise signals are sparse, meaning that only one noise signal is present at a given frequency. Multiple noise signals may be active at the same time, however, if a signal is not sparse in the frequency domain, then its mixing vector cannot be accurately estimated by cluster analysis. Compressive sensing also requires sparsity in order to accurately reconstruct the separate signals. Compressive sensing can fully reconstruct sparse signals, and approximately reconstruct near sparse signals. In this work, we do not exhaustively explore the minimum sparsity required for accurate reconstruction of the ambient magnetic field.

The proposed algorithm requires that several parameters be set by the user. In this study, the parameters were manually selected based on the signals being analyzed, but this process could also be automated. The first parameter is the quality factor, Q. This parameter adjusts the window size used in the Non-Stationary Gabor Transform. We experimentally selected it, but it may be chosen based on the length of the signal being processed. The parameter, λ, is used to remove low energy noise signals. Data points that are below a fraction, λ, of the maximum energy data point are removed before clustering occurs. We selected this parameter by analyzing the data projected onto the half-unit hypersphere in Figure 2, and visually observing if the signals were clusterable. If λ is too small, then the hypersphere will be completely filled with data points, and the noise signals will not be separable. If λ is too large, then small noise signals may not appear at all. Lastly, DBSCAN requires that two parameters, *eps*, and *MinPts*, be selected. The parameter, *eps*, represents the maximum distance allowed for two data points to be considered neighbors. The parameter, *MinPts*, represents the number of neighbors required for a data point to be considered a core. *MinPts* may be selected based on the length of signal being processed. A disadvantage of using NSGT and DBSCAN together is that more data points are created for higher frequency signals because the window size is altered based on frequency. Therefore, *MinPts* should be selected based on the lower frequency signals.

Most heliophysics missions require magnetic field accuracies of better than 1 nT (e.g., the NASA MMS mission [Russell et al., 2016]). The lowest error achieved in this experiment is 3.73 nT. This error is near the expected measurement noise for the PNI RM3100 magnetometer at 1 Hz, indicating that the accuracy of the algorithm is limited to the total error budget of the magnetometer. Nevertheless, the experiments performed show successful reconstruction of magnetic perturbation signals measured from within the bus of a mock CubeSat. These results demonstrate the utility of boomless CubeSats for scientific investigation of magnetic field phenomena in the geospace environment. In turn, the low cost of CubeSats enables the use of large constellations of small satellites to measure the geomagnetic field with high temporal and spatial resolution.

5 Conclusions and Future Work

In this study, we propose an algorithm for separating spacecraft generated magnetic noise from geomagnetic field data using multiple magnetometers. The algorithm does not require knowledge of the characteristics (location, orientation, amplitude, or spectral signature) and allows the number of noise sources to exceed the number of magnetometers ($n > m$). The algorithm identifies signals by looking at the relative gain and phase of the magnetometer data in the Time-Frequency domain. If a noise signal is sparse in this domain, the relative gain and phase is found using cluster analysis. Following the same assumption of sparsity, the signal can be separated from the noisy data using the cluster centroids in compressive sensing.

The algorithm is designed for underdetermined systems in which there are more noise sources than magnetometers. An advantage of this approach is that the UBSS algorithm can be integrated onto any satellite since no prior characterization of noise signals is required. This design eases the assimilation of magnetometers into spacecraft designs by reducing the need for strict magnetic cleanliness requirements and long mechanical booms.

There are several avenues of future development for this algorithm. The most immediate step to be taken is for the selection of parameters to be automated. We present an algorithm to automate the noise cancellation process, but some rudimentary analysis is still required to select parameters for clustering and pre-processing. We think the selection of parameters could be entirely automated. Another avenue of development is to test the limits of the sparsity assumption. Sparsity is a very strict assumption that may not always be met. In this work, we tested the algorithm using several wideband signals. However, the threshold for minimum sparsity is unknown. This assumption can be examined through examining signals with partially overlapping spectra to find a point of failure. Finally, an interesting scenario to investigate is where several magnetometers are mounted within the bus of a spacecraft, but one magnetometer is mounted on a short boom, such as on the spacecraft Dellingr (Kepko et al., n.d.). In this scenario, the measurements of one magnetometer may be more accurate than the others. It would be counterproductive if the reconstructed magnetometer signal had more noise than the signal measured by the magnetometer on the boom. It may be possible to account for this by designing a programmable "trust" parameter at the compressive sensing stage. This parameter would indicate an elevated degree of trust in one magnetometer over the others.

In this work, we performed two experiments to validate the algorithm. The first experiment separated SWARM magnetic perturbation data from four computer simulated signals. The algorithm was able to reconstruct the ambient magnetic field signal with an RMSE near 5 nT and a correlation of $\rho \approx 0.995$. The reconstruction errors are slightly less than the 6 nT intrinsic instrument noise that was added to each virtual magnetometer. The second experiment used real magnetic noise signals generated by copper coils, and the same SWARM geomagnetic field data. This experiment was able to separate four noise signals and reconstruct the background magnetic perturbation signal with a RMSE of 5.92 nT and a correlation of $\rho = 0.993$ at a 10 Hz cadence.

These results show the potential of signal processing algorithms to identify and remove magnetic noise from spaceborne magnetometer data. The proposed algorithm diminishes the need to place a magnetometer on a boom. This enables the possibility of low cost, boomless spacecraft to capture high fidelity magnetic field measurements.

Acknowledgments

This work was partially supported by NASA grants 80NSSC18K1240 and 80NSSC19K0608. The PNI RM3100 error estimates were provided by Dr. Lauro Ojeda. The SWARM perturbation data were provided by Dr. Yining Shi. The mock CubeSat used in this work was created by Dr. Srinagesh Sharma.

References

Baraniuk, R. G. (2007, July). Compressive Sensing [Lecture Notes]. *IEEE Signal Processing Magazine*, *24*(4), 118–121. (Conference Name: IEEE Signal Processing Magazine) doi: 10.1109/MSP.2007.4286571

Deshmukh, A. A., Sharma, S., Cutler, J. W., Moldwin, M., & Scott, C. (2020, February). Simple Regret Minimization for Contextual Bandits. *arXiv:1810.07371 [cs, stat]*. Retrieved 2021-07-23, from http://arxiv.org/

abs/1810.07371 (arXiv: 1810.07371)
Diamond, S., & Boyd, S. (n.d.). CVXPY: A Python-Embedded Modeling Language for Convex Optimization. , 5.
Domahidi, A., Chu, E., & Boyd, S. (2013, July). ECOS: An SOCP solver for embedded systems. In *2013 European Control Conference (ECC)* (pp. 3071–3076). Zurich: IEEE. Retrieved 2021-08-18, from https://ieeexplore.ieee.org/document/6669541/ doi: 10.23919/ECC.2013.6669541
Fratter, I., Léger, J.-M., Bertrand, F., Jager, T., Hulot, G., Brocco, L., & Vigneron, P. (2016). Swarm Absolute Scalar Magnetometers first in-orbit results. *Acta Astronautica*, *121*, 76–87. Retrieved from https://www.sciencedirect.com/science/article/pii/S0094576515004671 doi: https://doi.org/10.1016/j.actaastro.2015.12.025
Imajo, S., Nosé, M., Aida, M., Matsumoto, H., Higashio, N., Tokunaga, T., & Matsuoka, A. (2021, May). Signal and Noise Separation From Satellite Magnetic Field Data Through Independent Component Analysis: Prospect of Magnetic Measurements Without Boom and Noise Source Information. *Journal of Geophysical Research: Space Physics*, *126*(5). Retrieved 2021-06-30, from https://onlinelibrary.wiley.com/doi/10.1029/2020JA028790 doi: 10.1029/2020JA028790
Jaillet, F., Balazs, P., & Dorfler, M. (n.d.). Nonstationary Gabor Frames. , 4.
Kepko, L., Clagett, C., Santos, L., Azimi, B., Berry, D., Bonalsky, T., … Zesta, E. (n.d.). Dellingr: NASA Goddard Space Flight Center's First 6U Spacecraft. , 12.
Kilcommons, L. M., Redmon, R. J., & Knipp, D. J. (2017). A new DMSP magnetometer and auroral boundary data set and estimates of field-aligned currents in dynamic auroral boundary coordinates. *Journal of Geophysical Research: Space Physics*, *122*(8), 9068–9079. Retrieved 2021-11-02, from https://onlinelibrary.wiley.com/doi/abs/10.1002/2016JA023342 (_eprint: https://onlinelibrary.wiley.com/doi/pdf/10.1002/2016JA023342) doi: 10.1002/2016JA023342
Ludlam, M., Angelopoulos, V., Taylor, E., Snare, R. C., Means, J. D., Ge, Y. S., … Moreau, T. (2009). The THEMIS Magnetic Cleanliness Program. In J. L. Burch & V. Angelopoulos (Eds.), *The THEMIS Mission* (pp. 171–184). New York, NY: Springer. Retrieved 2022-01-31, from https://doi.org/10.1007/978-0-387-89820-9_8 doi: 10.1007/978-0-387-89820-9_8
McMahon, P., Jung, H.-J., & Edwards, J. (2013, September). Swarm Deployable Boom Assembly (DBA) Development of a Deployable Magnetometer Boom for the Swarm Spacecraft. , *718*, 13. Retrieved 2021-08-19, from https://ui.adsabs.harvard.edu/abs/2013ESASP.718E..13M (Conference Name: 15th European Space Mechanisms and Tribology Symposium ADS Bibcode: 2013ESASP.718E..13M)
Miles, D. M., Howarth, A. D., & Enno, G. A. (2019, August). In situ calibration of offsetting magnetometer feedback transients on the Cassiope spacecraft. *Geoscientific Instrumentation, Methods and Data Systems*, *8*(2), 187–195. Retrieved 2021-07-31, from https://gi.copernicus.org/articles/8/187/2019/ (Publisher: Copernicus GmbH) doi: 10.5194/gi-8-187-2019
Naik, G., & Kumar, D. (2009, December). Determining Number of Independent Sources in Undercomplete Mixture. *EURASIP J. Adv. Sig. Proc.*, *2009*. doi: 10.1155/2009/694850
Ness, N. F., Behannon, K. W., Lepping, R. P., & Schatten, K. H. (1971). Use of two magnetometers for magnetic field measurements on a spacecraft. *Journal of Geophysical Research (1896-1977)*, *76*(16), 3564–3573. Retrieved 2021-07-23, from https://agupubs.onlinelibrary.wiley.com/doi/abs/10.1029/JA076i016p03564 (_eprint: https://agupubs.onlinelibrary.wiley.com/doi/pdf/10.1029/JA076i016p03564)

doi: 10.1029/JA076i016p03564
Ream, J. B., Weiss, B. P., Oran, R., Raymond, C. A., Polanskey, C. A., Wenkert, D. D., ... Merayo, J. M. G. (2021, November). Magnetic gradiometry using frequency-domain filtering. *Measurement Science and Technology*, *33*(1), 015104. Retrieved 2022-01-14, from https://doi.org/10.1088/1361-6501/ac2e2e (Publisher: IOP Publishing) doi: 10.1088/1361-6501/ac2e2e
Regoli, L. H., Moldwin, M. B., Pellioni, M., Bronner, B., Hite, K., Sheinker, A., & Ponder, B. M. (2018, March). Investigation of a low-cost magneto-inductive magnetometer for space science applications. *Geoscientific Instrumentation, Methods and Data Systems*, *7*, 129–142. Retrieved 2021-11-25, from https://ui.adsabs.harvard.edu/abs/2018GI......7..129R (ADS Bibcode: 2018GI......7..129R) doi: 10.5194/gi-7-129-2018
Russell, C. T. (Ed.). (2004). *The Cassini-Huygens Mission: Orbiter In Situ Investigations Volume 2*. Dordrecht: Springer Netherlands. Retrieved 2022-01-31, from http://link.springer.com/10.1007/978-1-4020-2774-1 doi: 10.1007/978-1-4020-2774-1
Russell, C. T., Anderson, B. J., Baumjohann, W., Bromund, K. R., Dearborn, D., Fischer, D., ... Richter, I. (2016, March). The Magnetospheric Multiscale Magnetometers. *Space Science Reviews*, *199*(1), 189–256. Retrieved 2022-01-11, from https://doi.org/10.1007/s11214-014-0057-3 doi: 10.1007/s11214-014-0057-3
Sheinker, A., & Moldwin, M. B. (2016, February). Adaptive interference cancelation using a pair of magnetometers. *IEEE Transactions on Aerospace and Electronic Systems*, *52*(1), 307–318. (Conference Name: IEEE Transactions on Aerospace and Electronic Systems) doi: 10.1109/TAES.2015.150192
Sun, J., Li, Y., Wen, J., & Yan, S. (2016, January). Novel mixing matrix estimation approach in underdetermined blind source separation. *Neurocomputing*, *173*, 623–632. Retrieved 2021-08-17, from https://www.sciencedirect.com/science/article/pii/S092523121501142X doi: 10.1016/j.neucom.2015.08.008